This article has been accepted for publication in a future issue of this journal, but has not been fully edited. Content may change prior to final publication. Citation information: DOI 10.1109/LAWP.2018.2848912, IEEE Antennas and Wireless Propagation Letters

Compact and Low Cost 3D-Printed Antennas Metalized using Spray-Coating Technology for 5G mm-Wave Communication Systems

Shaker Alkaraki, Andre Sarker Andy, Yue Gao, Kin-Fai Tong, Zhinong Ying, Robert Donnan and Clive Parini

***Abstract*— This paper presents a design of two compact, light, rigid and low-cost 3D-printed millimeter-wave antennas for 5G communication system. The proposed antennas consist of a radiating slot that is surrounded by a rectangular cavity and corrugations which boost the gain performance of the antennas. Furthermore, the proposed antennas are fabricated using 3D-printing technology and they are metallized using novel, simple and low cost techniques which utilizes commercial conducive spray-coating technology. The proposed antennas operate at 28-GHz band, where the first design is fed by a waveguide to prove the performance, while the second design is fed by a microstrip line to demonstrate the ability to be integrated into a compact structure. Measurement results show a wide impedance bandwidth which enables the proposed antenna design to be a strong candidate for 5G applications.**

***Index Terms* – 3D-printed antenna, slot antenna, 28-GHz, 5G, grooves, corrugations, millimetre-wave (mm-wave).**

I. INTRODUCTION

Fifth generation (5G) mobile communications technology which is expected to be standardized by 2020 is a promising technology which is expected to achieve 1000 times overall system capacity, ten times data rate (i.e. peak data rate of 1 Gb/s for high mobility and 10 Gb/s for low mobility), 25 times average cell throughput, at least 10 times spectral and energy efficiency with 5 times lower latency. The main target of 5G technology is to connect the entire world and to achieve extremely reliable, robust and energy efficient communication between anything (machine to machine, people to machine) or anybody (person to person) [1]-[2]. Yet, 5G technology is not completely standardized, and several research activities are performed on different technologies, work on different frequency bands in a range of frequencies between 5 GHz to 70 GHz including the 28-GHz band [2-3]. Furthermore, the 28-GHz band was amongst the highlighted bands above 24 GHz to be used for future mobile communications by the Federal communication commission [4]. 3D-printing, also known as additive manufacturing (AM) is a promising technology that enables fast and cost-effective prototyping. Lately, several metal-plated, plastic 3D-printed antennas have been reported, where the plastic prototypes are covered by metal through the conventional plating or metallization techniques [5-8].

In this paper, we propose two small, compact, efficient and low cost 3D-printed antennas metalized using novel and simple techniques based on electromagnetic interference and also called radio frequency interference (EMI/RFI) conductive spray-paint technology. The proposed spray coating technology is used to metallize the 3D-printed plastic antenna instead of conventional metallization methods. The proposed metallization method reduces the cost of fabrication and it reduces the complexity of the fabrication process.

Shaker Alkaraki, Andre Sarker Andy, Yue Gao, Robert Donnan and Clive Parini are with the School of Electronic Engineering and Computer Science, Queen Mary University of London, London, E1 4NS, U.K. (e-mail: s.m.alkaraki, a.andy, yue.gao, r.donnan, c.g.parini @qmul.ac.uk). Kin-Fai Tong is with the department of electronic and electrical engineering, University College London, London, WC1E 7LE, U.K. (email: k.tong@ucl.ac.uk). Zhinong Ying is with Sony Mobile Communications,Mobilvägen1,SE22188,Lund,Sweden. (email:ying.zhinong@sonymobile.com).

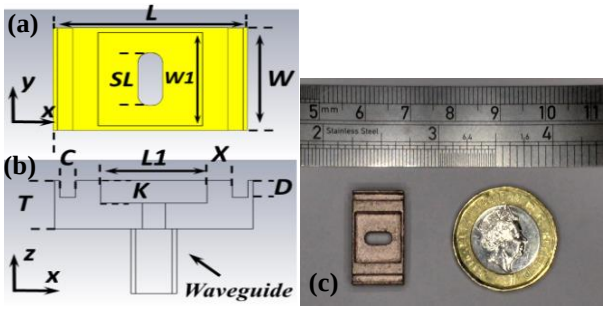

Fig.1 Schematics of Ant-1 (a) Top view, (b) cross section of front view and (c) fabricated prototype.

II. ANTENNA STRUCTURE AND FABRICATION METHOD

The first proposed antenna (Ant-1) consists of a resonant slot surrounded by a rectangular cavity and two corrugations. The rectangular cavity and the two corrugations improve the directivity and the gain of the antenna. In addition, the electromagnetic (EM) energy is coupled to the antenna surface using a standard rectangular waveguide by the means of resonant slot utilizing WR-28 (Ka-band) waveguide with dimensions of $a \times b = 7.112\,mm \times 3.556\,mm$. The waveguide length a is along the direction of slot length (SL), while the waveguide width is along the direction of slot width (SW). Hence, EM energy is coupled to the antenna surface along (SW) direction which makes the electric field (E-field) polarized along the x-direction. The optimized dimensions that maximize the directivity of the antenna at resonance frequency can be summarized as follows:

$$W1 \approx L1 \approx \lambda \quad (1), \quad K \approx \frac{\lambda}{3} \quad (2), \quad D \approx \frac{\lambda}{5} \quad (3)$$

where, λ is the resonance wavelength. The dimensions of the antenna are: antenna length $L = 20\,mm$, antenna width $W = 11\,mm$, slot length $SL = 5.7\,mm$, rectangular cavity length $L1 = 10.8$, plate thickness $T = 6.4\ mm$, rectangular cavity width $W1 = 10.6\,mm$, rectangular cavity depth $K = 3.2\,mm$, corrugation width $C = 1.6\,mm$, corrugation depth $D = 2.1\,mm$ and distance between cavity and corrugation $X = 2.6\,mm$. The proposed antenna is commonly fabricated using a metallic plate such as Aluminium and the corrugations and the slot are drilled using Computer Numerical Control (CNC) milling and micromachining [7]. However, fabricating such a structure using CNC milling requires advanced machinery and skilled labour and produces a relatively heavy metallic prototype. Hence, to simplify the fabrication procedure, the antenna is 3D-printed in house using a plastic material. The plastic material used is a transparent vero clear polyethelene which enables fabrication of a solid, rigid and light prototype with an overall weight of 1.35 grams for Ant-1 which is ~ 2-3 times lighter than an

This article has been accepted for publication in a future issue of this journal, but has not been fully edited. Content may change prior to final publication. Citation information: DOI 10.1109/LAWP.2018.2848912, IEEE Antennas and Wireless Propagation Letters

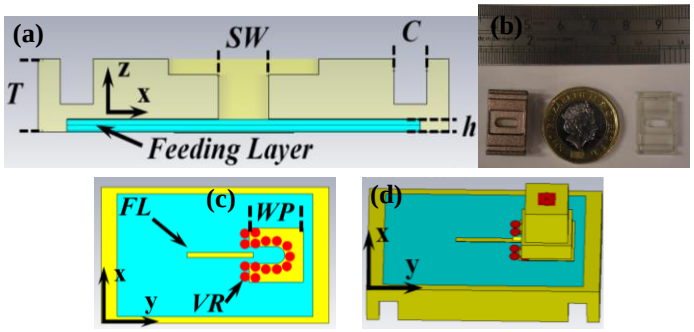

Fig.2. Schematic of Ant-2. (a) Cross section of front view, (b) fabricated prototype, (c) bottom view and (d) perspective bottom view with the connector. W = 10 mm, T = 3 mm, GW = 1.5 mm, L = 17 mm, Gd = 1.9 mm, h = 0.508 mm, W1 = 9.5 mm, L1 = 7 mm, X = 3.2 mm, SW = 2.2 mm, SL = 6.5 mm , FW = 0.4 mm, FL = 5.4 mm, VR = 0.8 mm, WP × WP = 4.4 mm × 4.4 mm.

Aluminum counterpart. A 3D-printer (Stratasys Objet30 Prime) is used to model the prototype as it prints with a layer thickness of 16 μm and a resolution of 100 μm. The prototype is 3D-printed with a clear finish and the support material used in the 3D-printing process effectively removed by rinsing the prototype using pressurized water. The cost of vero clear transparent polyethelene is ≈650 USD per kg. Hence, the cost of material including the support material used to 3D-print the prototype is less than 2 USD. Therefore, Objet30 offers cost-effective solutions to 3D-print small structures with high resolution for millimeter-wave applications. Then, the 3D-printed plastic prototype is metallized using a commercial and low cost conductive spray-paint that has superior scratch resistance characteristics with very strong adhesive properties on wide range of substrates [9]. This conductive metal spray constituent of metallic particles and acrylic resin along with compressed air. Two coats of the conductive spray paint are applied directly to the surface of the antenna at room temperature with less than one hour separation time between them. The paint typically dries within 5 minutes and it delivers maximum conductivity after 24 hours [9].

The schematic and the prototype of the second antenna (Ant-2) are shown in Fig. 2. Ant-2 is a smaller and a more compact version of Ant-1 due to a special microstrip feeding structure. Therefore, Ant-2 consists of two layers; the 1st layer is a feeding structure designed to feed the 2nd layer which is the 3D-printed radiating structure. As shown in Fig. 2(c); the feeding layer is designed to accommodate the PE 44489 mini-SMP connector. It consists of transmission line, mini-SMP pad (ground plane) and vias fabricated on Rogers RO4003C substrate using conventional PCB fabrication techniques to guarantee good performance. RO4003C is hydrocarbon ceramic laminate which has a dielectric constant of 3.38 and thickness of $h = 0.508\ mm$. The second layer of Ant-2 is the radiating structure and it is similar to Ant-1 as it contains a 3D-printed resonant slot surrounded by a rectangular cavity and two corrugations. The commercial spray used for spray-coating is RS EMI/RFI 400 ml Shielding Aerosol available commercially at a cost of ~50USD per 400ml can. Using spray-coating technology to metallize the proposed 3D-printed antenna over the conventional metallization techniques such as electro-less plating has several advantages such as a significant cost reduction as metallizing Ant-1 and Ant-2 using the proposed technique cost less than 2 USD for low volume prototyping since the aerosol has a large coverage area of ≈1.25 square meter per 400ml [9]. Hence, the overall cost

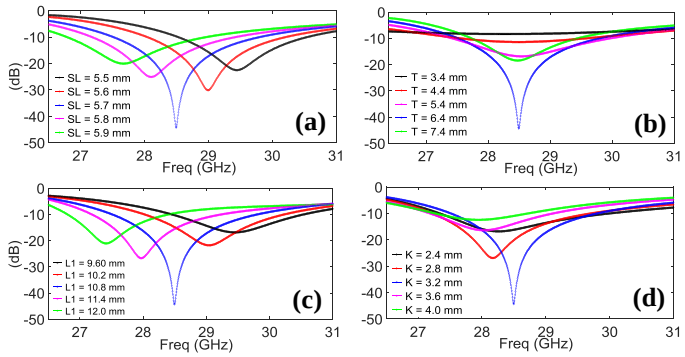

Fig.3. Effect of Ant-1 parameters on S_{11}. (a) SL, (b) T, (c) $L1$ and (d) K.

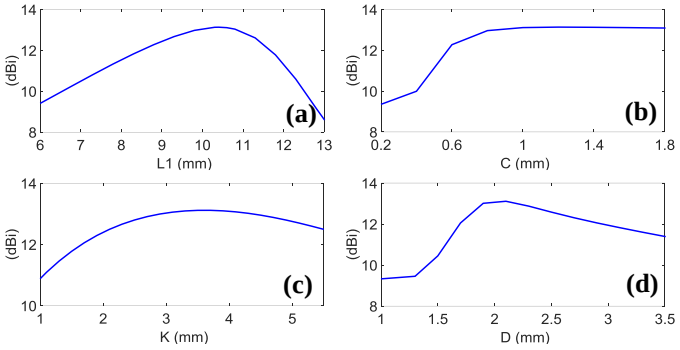

Fig.4 Effect of Ant-1 parameters on the directivity. (a) $L1$, (b) C, (c) K and (d) D.

of fabrication of the antenna is very low if compared to CNC milling or if electro-less plating is chosen as an alternative metallization technique. Furthermore, using spray-coating simplifies the fabrication procedure since the paint can be used at room temperature and the 3D-printed prototypes do not need any special pre-treatment or post-treatment process before or after spraying. In addition, the proposed spray-coating technique can be applied directly to open geometry structures such as Ant-1 and Ant-2, but it is not possible to be applied to complex and closed geometry structures, unless they are disassembled as in [10]. One of the main disadvantages of the proposed metallization technique that is not possible to effectively control its thickness uniformity across the whole structure. Therefore, two coats were primarily applied to make sure that the interior sides of the slot and corrugations are painted which makes the measured paint thickness on the surface of the prototype varying in the range of 45~65 μm, which is higher than the skin depth of copper ~0.39 μm at 28.5 GHz. Hence, more expensive and complex plating techniques such as electro-less plating [10] are recommended as a reliable alternative plating method, if the thickness of the metallization layer is highly critical.

III. Results and Analysis

A. Operating Principles

Ant-1 and Ant-2 share the same operating principles with a difference in the feeding method and the overall size, as Ant-2 has a smaller and a more compact size than Ant-1 with an overall thickness of 3 mm instead of 6.4 mm for Ant-1. For Ant-1 and Ant 2, the EM energy is coupled to the surface of the 3D-printed structure via resonant slot, where the resonance frequency of the slot is inversely proportional to its length ($SL \approx \frac{\lambda}{2}$) as shown in Fig. 3(a).

This article has been accepted for publication in a future issue of this journal, but has not been fully edited. Content may change prior to final publication. Citation information: DOI 10.1109/LAWP.2018.2848912, IEEE Antennas and Wireless Propagation Letters

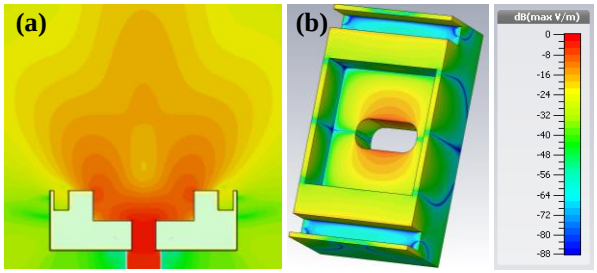

Fig.5 Power flow for Ant-1 at (x-z) cutting plane and E-field distribution on the surface of the antenna at 28.5 GHz. (a) Ant-1 power flow and (b) Ant-1 E-field.

Table.1. Comparison of the proposed antennas performance with PE –horn and 5G antennas at 28.5 GHz.

Antenna	Dimensions	Gain (dBi)	Bandwidth (%)	Ae (%)
Ant-1	$1.9\,\lambda \times 1.05\,\lambda \times 0.61\,\lambda$	12.4	8.8	70
Ant-2	$1.6\,\lambda \times 0.94\,\lambda \times 0.28\lambda$	8	12.9	33
Horn	$2.1\,\lambda \times 1.5\,\lambda \times 4.5\,\lambda$	13.5	≈ 40	59.5
[16]	$2.8\,\lambda \times 1.9\lambda \times 0.09\,\lambda$	7.5	≈ 8.7	8.3
[17]	$2.48\,\lambda \times 2\lambda \times 0.09\,\lambda$	12.7	≈ 20	30

The antennas offers high gain performance due to combined radiation from the slot, the rectangular cavity and the corrugations. For instance, in Ant-1, the used WR28 waveguide operates in the dominant transverse electric (TE_{10}) mode and it couples the EM energy to the surface of the antenna, where part of this energy is radiated by the slot and the rest of the coupled energy is converted to a travelling-wave that propagates in the x-direction on the surface of the antenna and ultimately lost and leaked at antenna edges. Hence, Ant-1 has a directivity of 5.6 dBi once the slot is solely present on the surface of the 3D-printed structure and this is due to conventional space-wave radiaton from the slot. However, the directivity of the antenna is boosted by an extra ~3 dBi once the corrugations are added and by further 4.4 dBi once the rectangular cavity is added. In fact, both the rectangular cavity and the corrugations excite the travelleing-wave on the surface of the antenna resulting in an improvement in the directivity and gain performance of the antenna resulting in combined radiation in the boresight. Hence, the peak directivity performance is obtained once the dimensions of the cavity and the corrugations are optimized as shown in Fig.4. Moreover, the reason behind the gain improvement in the proposed antenna after the introduction of the rectangular cavity on the surface of the antenna is due to the radiation caused by the cavity due to strong excitaiton and resonance of the dominant (TM_{12}) mode inside the cavity as shown in Fig.5 (b). Hence, the length of the cavity $L1$ has a major effect on the resonance frequency of the antenna as shown in Fig.3 (a). Also, $L1$ has an effect on the directivity of the antenna as the peak in the directivity is obtained once $L1$ is equivalent to λ. Furthermore, the depth of the cavity K affects the performance of the antenna as shown in Fig. 3(d) and Fig. 4(c). For instance, the directivity sees a major improvement once K is larger than quarter wavelength ($K = \frac{\lambda}{4} = 2.6\,mm$) with a directivity of 12.7 dBi, and the maximum directivity of 13.2 dBi is obtained once K is in range of $\frac{3\lambda}{10} \leq K \leq \frac{4\lambda}{10}$ as shown in Fig.4 (c), hence in the proposed design of Ant-1, K is set to $\frac{3\lambda}{10} = 3.2\,mm$ at 28.5 GHz. In addition, the two corrugation contributes to a further ~3 dBi improvements in the directivity of the antenna due to excitaition of the EM waves on the

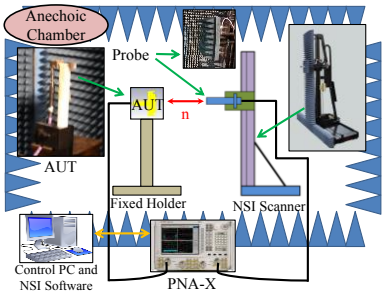

Fig. 6. The measurement setup used to measure the proposed antennas. The distance between probe and antenna under test is n ≈ 4.2λ.

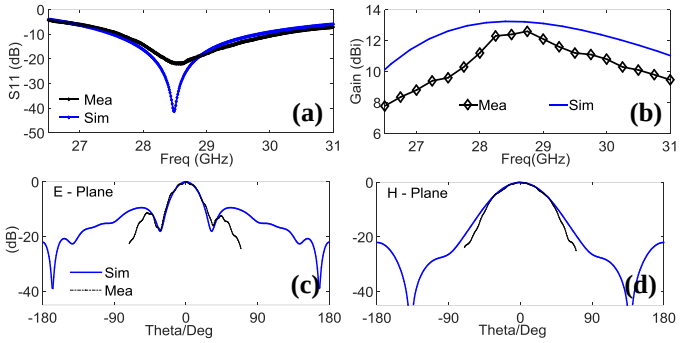

Fig.7. Measured and simulated results of Ant-1. (a) S_{11}, (b) gain, (c) E-plane, and (d) H-plane at 28.5 GHz.

surface of the antenna as analyzed in [11-15]. Furthermore, the main tradeoff of adding the cavity to the surface of Ant-1 with a depth of $K \approx \frac{\lambda}{3}$ is that the overall thickness of the antenna has to be increased. However, even with the cavity, Ant-1 is compact and it has a superior aperture efficiency performance compared to the dimensions of other antennas with similar feeding structure such as PE 9850-15 standard horn or if compared to 5G antennas presented in [16] and [17].

B. *EXPERIMENTAL AND NUMERICAL RESULTS*

Ant-1 and Ant-2 are numerically analyzed using CST microwave studio software and the prototypes are fabricated and tested. Both structures were simulated as a perfect electric conductor (PEC) with an extremely smooth surface. The reflection coeficient is experimentally measured using a vector network analyzer, while the the gain of the antennas has been measured using the standard horn gain comparison method described in detail in [18]. Moreover, the gain and far-field radiation patterns were measured using near field scanning. The system which has been used to measure the antenna near-field is (200V NSI). 200V NSI is a vertical planar scanner, where it has been used with the measurement setup provided in Fig. 6. The proposed antenna (AUT) is mounted on top of a stationary holder and the near-field probe raster scan in the X and Y direction along the surface of the antenna, so that samples of the near-field are measured. The separation between the AUT and the probe is recommended to be in range of $3\lambda \leq n \leq 5\lambda$. This separation is chosen to maximize the angular range over which the far-field data is reliable [19]. The measured results shows that Ant-1 resonates at 28.5 GHz with a measured bandwidth of 2.5 GHz (8.8%) compared to a 2.3 GHz bandwidth in the simulation as shown in Fig.7 (a). The proposed antenna has a peak measured gain of 12.5 dBi at 28.7 GHz and a gain of 12.4 dBi at 28.5 GHz as shown in Fig.7.(b), compared to a simulated gain of 13.2 dBi at 28.5 GHz. It is also observed, from Fig.7 (b), that the measured gain is more than 10 dBi over the entire bandwidth of the antenna and the gain is particularly higher than 12 dBi over

This article has been accepted for publication in a future issue of this journal, but has not been fully edited. Content may change prior to final publication. Citation information: DOI 10.1109/LAWP.2018.2848912, IEEE Antennas and Wireless Propagation Letters

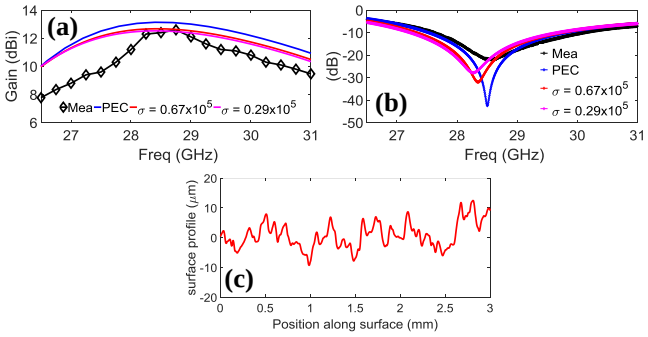

Fig.8. The effect of conductivity on the gain and the S_{11} of Ant-1 and surface profile measurements. (a) Gain, (b) S_{11} , (c) Ant-1 surface profile along the surface of the antenna after spraying.

800 MHz of the operating bandwidth. Besides, Ant-1 has a half power beam width (HPBW) of 30° with side lobe level (SLL) of -12 dB in the E-plane and HPBW of 54° in the H-plane and with front to back (F/B) ratio of 20.1 dB. In addition, one of the main figure of merits of Ant-1 is its compact size and high measured aperture efficiency (A_e). A_e is defined as the ratio of the maximum effective antenna aperture area to its physical aperture area and it determines how efficiently the physical area of the antenna is utilized [20]. The outstanding A_e performance of Ant-1 is due to its high gain performance compared to its small size. Ant-1 has an A_e of 70% at 28.5 GHz and A_e approaches a peak of 71.7% at 28.7 GHz. In comparison to an A_e of 59.5% for PE 9850-15 horn, 8.3% to the 28.5 GHz tilted beam 5G antenna fed by waveguide and to an A_e of 30% at for 5G Franklin array that has been presented recently in [17]. A detailed comparison between the proposed antennas performance with other antennas is shown in Table.1. Furthermore, Ant-1 is compact once compared to the Ka-band PE 9850-15 horn as the horn is 7.4 times higher than Ant-1 with an overall height of 4.5 λ at 28.5 GHz as compared to only 0.61λ incase of Ant-1. Generally, the measured gain of Ant-1 is in range of 0.7 dB to 2 dB lower than the simulated gain as shown in Fig. 7(b), while the measured bandwidth is 200 MHz wider than the simulated one. In fact, the lower gain and wider bandwidth are mainly due to the conduction losses introduced by the paint as shown in Fig.8 (a) and (b). The paint has a surface resistivity of $R_s = 0.3 - 0.7\ \Omega/\square$ at 50 μm thickness [9], which makes its conductivity $\sigma = 0.29 \times 10^5 - 0.67 \times 10^5\ S/m$. This contributes to a gain losses of $0.4 \sim 0.8$ dB at 28.5 GHz compared to PEC as the simulation results shows in Fig.8(a). Hence, at 28.5 GHz the antenna simulated gain is 13.2 dBi for PEC, 12.7 dBi for $\sigma = 0.67 \times 10^5\ S/m$ and 12.5 dBi for $\sigma = 0.29 \times 10^5\ S/m$ which is 0.1 dBi higher than the measured gain. Furthermore, fabrication tolerances and non-uniformity of the thickness of the paint might affect the S_{11} performance of the antenna as the paint thickness was not counted for in the simulation process, especially that the resonance frequency is sensitive to the dimensions of the slot as shown in Fig.3.(a). However, the surface roughness of the paint is hardly responsible for any gain losses. The surface profile measurement of the antenna after applying the paint using a Profilometer is shown in Fig.8(c). The measured root mean square (RMS) roughness of the paint at antenna surface is 4.92 μm along a path of 3 mm. However, it has been reported in [21] that a surface roughness of 25.9 μm (RMS) has no effect on the gain of a Ku-band horn antenna at 15 GHz, while a

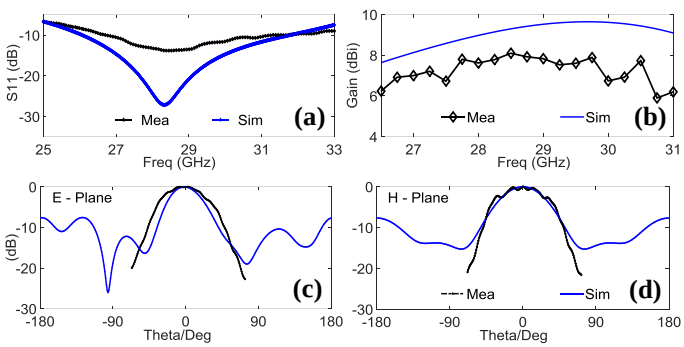

Fig.9. Measured and simulated results of Ant-2. (a) S_{11}, (b) gain, (c) H-plane and (d) E-plane at 28.5 GHz.

measured ~0.7 dB loss in the horn gain is noticed once it has an extreme surface roughness of 39.7 μm (RMS) which is noticeably far larger than the proposed antenna surface roughness. Furthermore, the measured and simulated reflection coefficient of Ant-2 is shown in Fig. 9(a) and it shows that the measured -10 dB bandwidth of the antenna is 3.7 GHz (12.9%) ranges from 26.9 GHz to 30.6 GHz. Furthermore, Ant-2 has a simulated peak gain of 9.6 dBi at 29.5 GHz and a simulated gain of 9.4 dBi at 28.5 GHz. However, the measured peak gain is 8 dBi at 28.5 GHz and 7.9 dBi at 29.5 GHz and the antenna measured gain is higher than 7.6 dBi over 2 GHz bandwidth, ranges from 27.7 GHz to 29.7 GHz as shown in Fig.9 (b). The simulated and measured far-field radiation patterns of the antenna at 28.5 GHz are shown in Fig. 8. The proposed antenna has a measured HPBW of 60° in the H-plane and 53° in the E-plane, while the (F/B) ratio of the proposed antenna is 9.2 dB. The discrepancies between the simulated and measured results of Ant-2, besides the conduction losses as discussed in Ant-1 case, are due to insertion losses as well as matching losses due to mini-SMP connector soldering and misalignment with the 0.4 mm width transmission line and fabrication tolerances of the feeding layer. Finally, in Ant-2, the EM energy is coupled via the mini-smp connector to the transmission line in the feeding structure. Then, the EM waves are coupled from the transmission line to the surface of the 3D-printed structure via the slot and the introduction of the cavity and the corrugations excites the EM waves on the surface of the antenna and the combined radiation from the slot, cavity and corrugations is responsible for the gain enhancement in similar manner to Ant-1. Therefore, the antenna has a gain of 4.9 dBi at 28.5 GHz due to radiation from the slot only and a peak gain of 8.7 dBi with the corrugations and 9.6 dBi with the corrugations and cavity.

IV. Conclusion

This paper presents designs of efficient, high gain and compact 3D-printed antennas metalized using low-cost EMI/RFI spray-coating technology. Using EMI/RFI conductive paint reduces the production cost of the antenna and the complexity of the fabrication procedure, while delivering suitable performance at 28 GHz band. Finally, the novel fabrication method employed in this investigation, offers the proposed antenna to be a potential candidate for low-cost 5G mm-wave applications.

This article has been accepted for publication in a future issue of this journal, but has not been fully edited. Content may change prior to final publication. Citation information: DOI 10.1109/LAWP.2018.2848912, IEEE Antennas and Wireless Propagation Letters

References

[1] Ericsson.com, "Mobility Report," 2015. [online], available: http://www.ericsson.com/res/docs/2015/ericsson-mobility-report-june-2015.pdf. [Accessed: 5th – Jan - 2018].

[2] NTT Docomo Inc., "NTT DOCOMO's Views on 5G," Presentation, 2014,available:http://johannesbergsummit.com/wp-content/uploads/sites/6/2013/11/Nakamura-Johnnesberg-Summit-NTT-DOCOMOs-Views-on-5G_rev.pdf [Accessed: 5th – Jan - 2018].

[3] S. F. Jilani and A. Alomainy, "Millimetre-wave T-shaped MIMO antenna with defected ground structures for 5G cellular networks," *IET Microwaves, Antennas & Propagation*, vol. 12, no. 5, pp. 672-677, 2018.

[4] Use of Spectrum Bands above 24 GHz for Mobile Radio Services, GN Docket No. 14-177, Notice of Proposed Rulemaking, 15 FCC Record 138A1 (rel. Oct. 23, 2015).

[5] G. P. Le Sage, "3D Printed Waveguide Slot Array Antennas," *IEEE Access*, vol. 4, no. , pp. 1258-1265, 2016.

[6] J. A. Gordon *et al*., "An All-Metal, 3-D-Printed CubeSat Feed Horn: An assessment of performance conducted at 118.7503 GHz using a robotic antenna range.," *IEEE Antennas and Propagation Magazine*, vol. 59, no. 2, pp. 96-102, April. 2017.

[7] U. Beaskoetxea, S. Maci, M. Navarro-Cía and M. Beruete, "3-D-Printed 96 GHz Bull's-Eye Antenna With Off-Axis Beaming," *IEEE Transactions on Antennas and Propagation*, vol. 65, no. 1, pp. 17-25, Jan. 2017.

[8] Y. Tawk, M. Chahoud, M. Fadous, J. Costantine and C. G. Christodoulou, "The Miniaturization of a Partially 3D Printed Quadrifilar Helix Antenna," in *IEEE Transactions on Antennas and Propagation*, vol. PP, no. 99, pp. 1-1.

[9] RS EMI/RFI Shielding Aerosol with Bronze colour 400mL data Sheet , https://docs-emea.rs-online.com/webdocs/1583/0900766b8158361e.pdf Accessed: 20th – April – 2018].

[10] M. D'Auria *et al*., "3-D Printed Metal-Pipe Rectangular Waveguides," *IEEE Transactions on Components, Packaging and Manufacturing Technology*, vol. 5, no. 9, pp. 1339-1349, Sept. 2015.

[11] S. Alkaraki, Yue Gao and C. Parini, "High aperture efficient antenna at Ku band," *2017 International Workshop on Electromagnetics: Applications and Student Innovation Competition*, London, 2017, pp. 60-62.

[12] D. Y. Na, K. Y. Jung and Y. B. Park, "Transmission Through an Annular Aperture Surrounded With Corrugations in a PEC Plane," in *IEEE Antennas and Wireless Propagation Letters*, vol. 14, pp. 179-182, 2015.

[13] S. Alkaraki, Y. Gao and C. Parini, "Dual-Layer Corrugated Plate Antenna," in *IEEE Antennas and Wireless Propagation Letters*, vol. 16, pp. 2086-2089, 2017.

[14] M. B. Diaz *et al*., "Dual-band low-profile corrugated feeder antenna," *IEEE Transactions on Antennas and Propagation*, vol. 54, no. 2, pp. 340-350, Feb. 2006.

[15] S. Alkaraki, Y. Gao and C. Parini, "Small and high gain millimetre wave corrugated grooves antenna," *2015 IEEE International Symposium on Antennas and Propagation & USNC/URSI National Radio Science Meeting*, Vancouver, BC, 2015, pp. 2091-2092.

[16] J. S. Park, J. B. Ko, H. K. Kwon, B. S. Kang, B. Park and D. Kim, "A Tilted Combined Beam Antenna for 5G Communications Using a 28-GHz Band," *IEEE Antennas and Wireless Propagation Letters*, vol. 15, pp. 1685-1688, 2016.

[17] S. F. Jilani and A. Alomainy, "A Multiband Millimeter-Wave 2-D Array Based on Enhanced Franklin Antenna for 5G Wireless Systems," in *IEEE Antennas and Wireless Propagation Letters*, vol. 16, pp. 2983-2986, 2017.

[18] Constantine A. Balanis,"Antenna Measurement",in Antenna Theory, 3rd ed. Hoboken, New Jersey: John Wiley and Sons, 2005, ch. 17, sec.4.2, pp. 1033-1034.

[19] Stuart Gregson, John McCormick and Clive Parini, "Principles of Planar Near-Field Antenna Measurements". Institution of Engineering and Technology, IET Electromagnetic Waves Series, 2007, Volume 53.

[20] Constantine A. Balanis, "Aperture Antennas", in Antenna Theory, 3rd ed. Hoboken, New Jersey: John Wiley and Sons, 2005, ch. 12, sec.5.3,pp. 682.

[21] C. R. Garcia, R. C. Rumpf, H. H. Tsang and J. H. Barton, "Effects of extreme surface roughness on 3D printed horn antenna," *Electronics Letters*, vol. 49, no. 12, pp. 734-736, June. 2013.